Optics Letters

Optical amplification-free deep reservoir computing-assisted high-baudrate short-reach communication

Mengyao Han,[1,2] Muguang Wang,[1,*] Yuchuan Fan,[3] Toms Salgals,[4,5] Hadrien Louchet,[6] Richard Schatz,[2] Markus Gruen,[6] Fabio Pittala,[6] Benjamin Krüger,[6] Thomas Dippon,[6] Lu Zhang,[7] Xianbin Yu,[7] Sandis Spolitis,[4,5] Vjaceslavs Bobrovs,[4] Sergei Popov,[2] Xiaodan Pang,[2,3,8] and Oskars Ozolins[2,3]

[1]Institute of Lightwave Technology, Key Lab of All Optical Network & Advanced Telecommunication Network, Ministry of Education, Beijing Jiaotong University, Beijing 100044, China
[2]Department of Applied Physics, KTH Royal Institute of Technology, 106 91 Stockholm, Sweden
[3]RISE Research Institutes of Sweden, 164 40 Kista, Sweden
[4]Institute of Telecommunications, Riga Technical University, 1048 Riga, Latvia
[5]Communication Technologies Research Center, Riga Technical University, 1048 Riga, Latvia
[6]Keysight Technologies GmbH, Böblingen, Germany
[7]College of Information Science and Electronic Engineering, Zhejiang University and Zhejiang Lab, Hangzhou, China
[8]xiaodan@kth.se
*mgwang@bjtu.edu.cn

Received 30 January 2023; revised 16 March 2023; accepted 17 March 2023; posted 17 March 2023; published 12 April 2023

An optical amplification-free deep reservoir computing (RC)-assisted high-baudrate intensity modulation direct detection (IM/DD) system is experimentally demonstrated using a 100G externally modulated laser operated in C-band. We transmit 112 Gbaud 4-level pulse amplitude modulation (PAM4) and 100 Gbaud 6-level PAM (PAM6) signals over a 200-m single-mode fiber (SMF) link without any optical amplification. The decision feedback equalizer (DFE), shallow RC, and deep RC are adopted in the IM/DD system to mitigate impairment and improve transmission performance. Both PAM transmissions over a 200-m SMF with bit error rate (BER) performance below 6.25% overhead hard-decision forward error correction (HD-FEC) threshold are achieved. In addition, the BER of the PAM4 signal is below the KP4-FEC limit after 200-m SMF transmission enabled by the RC schemes. Thanks to the use of a multiple-layer structure, the number of weights in deep RC has been reduced by approximately 50% compared with the shallow RC, whereas the performance is comparable. We believe that the optical amplification-free deep RC-assisted high-baudrate link has a promising application in intra-data center communications.

https://doi.org/10.1364/OL.485830

With the rapid development of large-scale data center networks, the emerging traffic has imposed stringent requirements on almost all aspects of short-reach optical communications to support the upcoming 800 Gbit/s and 1.6 Tbit/s Ethernet [1]. Intensity modulation and direct detection (IM/DD) systems fulfill the ever-growing traffic demand while keeping a low cost, low energy consumption, and small footprint. Currently, IM/DD systems with 200 Gbit/s/lane rate are considered strong candidates for intra-data center communications [2]. In addition, the IM/DD systems with parallel fibers or wavelength-division multiplexing (WDM) are competitive solutions to achieve 800 Gbit/s and beyond [3]. Recently, several short-reach optical transmission schemes have been reported in both O-band (i.e., 1.3 μm) and C-band (i.e., 1.55 μm). In [4], a 4×100 Gbit/s IM/DD system with four-level pulse amplitude modulation (PAM4) format over a 40-km single-mode fiber (SMF) transmission was demonstrated in the O-band. Up to 363 Gbit/s eight-level PAM (PAM8) and 279 Gbit/s polybinary transmissions over 10-km SMF were achieved using a plasmonic Mach–Zehnder modulator working at the C-band [5]. Considering the energy consumption and footprint requirements, these IM/DD systems would preferably operate with a monolithically integrated transceiver, e.g., vertical-cavity surface-emitting laser (VCSEL), directly modulated laser (DML) [6], and externally modulated laser (EML), as well as without any optical amplification [7]. In this case, various advanced digital modulation formats, including 100 Gbaud PAM4, 80 Gbaud PAM8, and 50 GHz bandwidth DMT signals, with a maximum bit rate of 236 Gbit/s were demonstrated with a 50G-class O-band DML [6]. In [7], 200 Gbaud on–off keying (OOK), 112 Gbaud PAM4, and 100 Gbaud 6-level PAM (PAM6) signals were transmitted over a few-hundred-meters SMF without any optical amplification using a 100G EML operated in the C-band, because of the optical modulated signals with the higher output power and the enhanced extinction ratio.

Despite operating at the O-band, the chromatic dispersion (CD)-induced power fading on the side channels of either LAN-WDM4/8 or Coarse WDM4/8 configurations arises as a critical issue at high-baudrate [8]. The capacity-distance product of the

IM/DD system is restricted by the CD-induced power fading [9]. Such an issue can be tackled by increasing the system power budget with higher output power from the transmitter and/or higher receiver sensitivity or using sophisticated mitigation methods in analog or digital domains [10]. In the digital domain, digital signal processing (DSP) algorithms, such as feedforward equalizer, decision-feedback equalizer (DFE), and nonlinear equalizations with Volterra series, etc., have been well studied and often used to mitigate the high-baudrate short-reach transmission impairments, i.e., CD-induced power fading, limited bandwidth, modulation nonlinearity, etc. [11]. Recently, the research community has also turned to machine-learning techniques, which bring opportunities to generate new knowledge in application to combat fundamental and practical challenges in optical communications [12]. Reservoir computing (RC) gains more attention due to many conspicuous advantages by virtue of its unique structure [13]. In addition, the optoelectronic or photonic RC, with the potential benefits of low power consumption and high-speed computation, has also been proposed to address signal recovery in optical communications [14,15].

In this Letter, we experimentally demonstrate an optical amplification-free high-baudrate IM/DD system using a 100G EML operated in the C-band. The transmissions of 112 Gbaud PAM4 and 100 Gbaud PAM6 signals were achieved over a 200-m SMF without any optical amplification. The DFE, shallow RC, and deep RC are adopted to mitigate link impairments. The BER performances of PAM4 and PAM6 signals below 6.25% overhead hard-decision forward error correction (6.25% OH HD-FEC) limit of 4.5×10^{-3} are obtained. In addition, we achieve the BER below the KP4-FEC limit of 2.2×10^{-4} in the PAM4 signal over 200-m SMF transmission, thanks to the performance improvement of RC schemes. The corresponding eye diagrams are also shown to verify the transmission performance. Finally, the computational complexity of these methods is also comparatively discussed. We believe the proposed optical amplification-free deep RC-assisted high-baudrate IM/DD system can provide a valuable reference for intra-data center communications.

Figure 1 shows the experimental setup and digital signal processor (DSP) routines for 112 Gbaud PAM4 and 100 Gbaud PAM6 transmissions. The PAM4 and PAM6 signals are generated in MATLAB. We first generate a pseudorandom bit sequence (PRBS) of >1 million bits using the Mersenne Twister generator with a shuffled seed number. Next, the PAM4 and PAM6 symbols are mapped from the PRBS and filtered by a root-raised-cosine filter with a 0.02 and 0.15 roll-off factor, respectively. Then, the pre-equalization is used to compensate for the bandwidth limitation of the IM/DD system, and PAM4

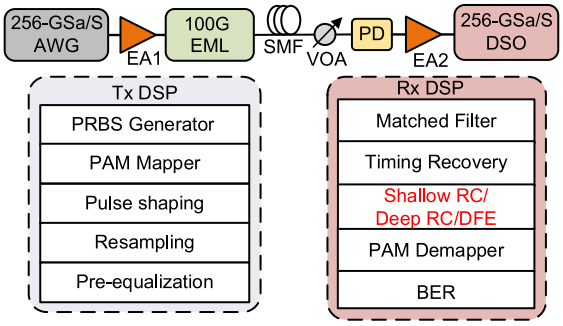

Fig. 1. Experimental setup and DSP routine in transmitter and receiver.

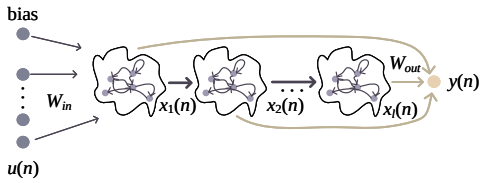

Fig. 2. Schematic diagram of the deep RC.

and PAM6 symbols are unsampled to 256 GSa/s to match the arbitrary waveform generator (AWG). After that, the output of the AWG signal is amplified by an electrical amplifier (EA1) with 60-GHz bandwidth. A C-band EML is used as an optical transmitter which consists of a monolithically integrated distributed feedback laser and traveling-wave electroabsorption modulator (DFB-TWEAM) [16]. The modulated signal's optical power at the output of the EML is 3.3 dBm, and the bandwidth of the EML is 100 GHz. After a 200-m SMF link, the received optical signal is sent to a photodetector (3-dB bandwidth > 90 GHz and responsivity = 0.5 A/W). A variable optical attenuator is used to adjust the received optical power (ROP) before the photodetector for transmission performance measurement. Then, the output of the photodetector is amplified by EA2 with 65-GHz bandwidth and sampled with a 256 GSa/s digital storage oscilloscope. In the DSP routine at the receiver, the DFE, shallow RC, and deep RC schemes are off-line achieved in the lab computer and used to mitigate the link impairment caused by the limited system bandwidth and modulation nonlinearity. After optimization of the number of taps, the DFE is configured at the 55 feedforward taps and 13 feedback taps [7], which benchmarks the BER performance of RC schemes. The DFE with adaptive weights is achieved by the least mean square algorithm.

Figure 2 shows the architecture of the deep RC. In the deep RC, the first layer is fed by the external input, whereas the output of the previous one feeds each successive layer. Note that we focus on the architecture whose all layers connect to the output layer. The reservoir state for each layer $x_l(n)$ can be obtained by the following function [17]:

$$x_l(n)=\begin{cases}\tanh(W_{in,1}u(n)+\theta_1+W_1x_1(n-1)) & l=1\\ \tanh(W_{in,l}x_{l-1}(n)+\theta_l+W_lx_l(n-1)) & l>1\end{cases}, \quad (1)$$

where tanh is the activation function, $u(n)$ is the input for the first layer, and θ_l is the bias-to-reservoir weight for the lth layer. Here, $W_{in,l}$ is the input weight for the lth layer and is selected from the uniform distribution over $[-\alpha, +\alpha]$, where α is the scale factor. The recurrent weight W_l for the lth layer is randomly generated from a uniform distribution and re-scaled according to the spectral radius ρ ($\rho<1$). The output of the deep RC is obtained by

$$y(n)=W'_{out}[u(n),x_1(n),x_2(n),x_3(n),\ldots,x_{NL}(n)]+\theta'_{out}, \quad (2)$$

where W'_{out} denotes the readout weight of the deep RC, which is decided in the training phase using the ridge regression algorithm, and θ'_{out} is the bias-to-readout weight. Note that the shallow RC can be achieved by setting $l=1$, and the input and output bias equals to 1. We collect the received symbols as our datasets for both RC schemes. The datasets of PAM4 and PAM6 have 870,000 and 840,000 symbols for each ROP, respectively. We first use 5% of dataset symbols in the training phase to calculate the weights. The weights are fixed after the training phase. After that, 5% of dataset symbols are chosen for validation to

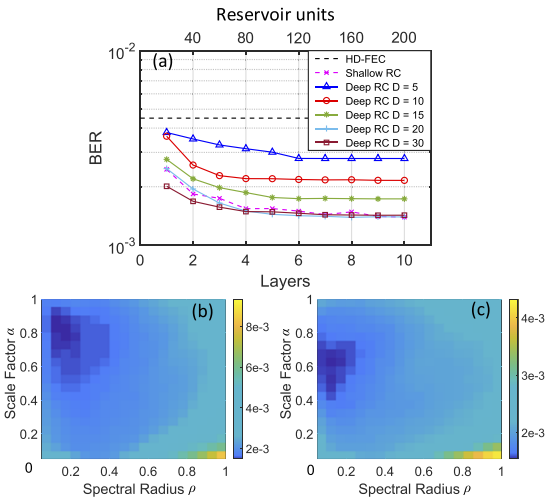

Fig. 3. (a) PAM6 BER versus the number of reservoir units or layers; relationship among the PAM6 BER, scale factor α and spectral radius ρ in (b) shallow RC and (c) deep RC.

optimize the RC performance. Finally, 90% of dataset symbols are selected to test the RC performance.

We first study the BER performance with the hyperparameters of shallow and deep RCs. An example of optimization is shown using PAM6 symbols after 200-m SMF transmission, and the optimization process for others is similar. The influence of the number of reservoir units and layers for 100 Gbaud PAM6 transmission over 200-m SMF is investigated. For this evaluation, we set scale factor $\alpha = 0.6$ and spectral radius $\rho = 0.1$ in shallow RC, scale factor $\alpha = 0.85$ and spectral radius $\rho = 0.1$ for all layers in deep RC, and regularization parameter $k = 1 \times 10^{-8}$ for both RCs. Figure 3(a) shows the relationship between the number of reservoir units or layers and 100 Gbaud PAM6 BER performance after 200-m SMF transmission. One can observe that the BER performance improves as the number of reservoir units grows for the shallow RC-based scheme. The BER floor occurs when the reservoir units are larger than 150. With fixed reservoir units D in each layer of deep RC, the BER performance of the PAM6 signal is improving as the number of layers L increases. With the same BER performance, the number of layers and the number of reservoir units in each layer can be optimized considering the computational complexity. To trade off the BER performance and the computational complexity of RC methods, we choose 80 reservoir units for shallow RC and 4 layers with 20 reservoir units in each layer for deep RC in the PAM6 transmission.

Then, we move to the optimization of scale factor α and spectral radius ρ in both RC approaches. The remaining parameters of RC are untouched. Figures 3(b) and 3(c) show the BER performance dependency on scale factor α and spectral radius ρ in shallow RC and deep RC, respectively. When the scale factor α and spectral radius ρ ranges from 0 to 1, we obtain BER $= 1.54 \times 10^{-3}$ around the region of $\alpha = 0.1$ and $\rho = 0.6$ for shallow RC and BER $= 1.5 \times 10^{-3}$ around the area of $\alpha = 0.1$ and $\rho = 0.85$ for deep RC. After the optimization of scale factor α and spectral radius ρ, the influence of the regularization parameter k is also evaluated, and the optimal regularization parameters of deep RC and shallow RC are 1×10^{-10} and 1×10^{-9}, respectively.

Next, 100 Gbaud PAM6 transmission performances are evaluated for the back-to-back (B2B) case and after 200-m SMF transmission. Figures 4(a) and 4(b) show the PAM6 BER as a function of ROP in the B2B case and after 200-m SMF transmission, respectively. By applying the RC and DFE approaches, BERs below 6.25% OH HD-FEC are achieved in both cases. BERs cannot meet the 6.25% OH HD-FEC requirements in both cases without the impairment mitigation schemes. Compared with the DFE, RC methods offer approximately 1-dB ROP sensitivity improvement at 6.25% OH HD-FEC in the B2B case and after 200-m SMF transmission. The selected eye diagrams with deep RC (left) and without post-processing (right) are shown in the insets of Figs. 4(a) and 4(b). In addition, 112 Gbaud PAM4 transmission performance is also evaluated after 200-m SMF transmission. Figure 4(c) shows the PAM4 BER as a function of ROP after 200-m SMF transmission. With the DFE, a BER performance below 6.25% OH HD-FEC is achievable, though BER performance below KP4-FEC is not achieved.

Further improvement in the BER performance can be obtained using RC approaches with 120 reservoir units for shallow RC and 30 reservoir units of four layers for deep RC. A PAM4 BER performance below KP4-FEC is achieved. Compared with the DFE, the RC schemes only bring limited improvement because the performance is mainly determined by the system noise for PAM signals. The selected eye diagrams with deep RC (left) and without post-processing (right) are also shown in the insets of Fig. 4(c) to show the transmission performance.

Finally, the computational complexity of RC approaches is compared. The number of weights often corresponds to the computational complexity (i.e., multiply operation, generation, storage of weights, etc.). Figure 5 shows the relationship between the number of weights and the number of reservoir units in shallow and deep RCs. One can see that the increase of weights

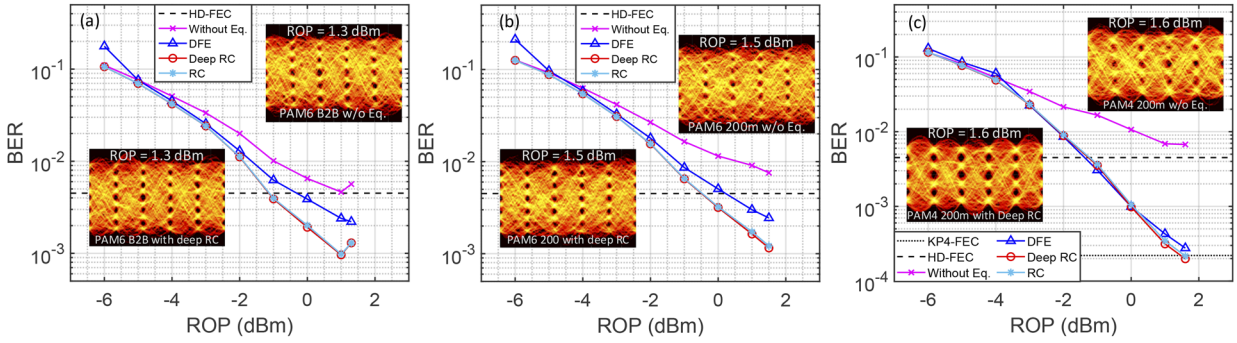

Fig. 4. (a) PAM6 BER versus ROP in the B2B case; (b) PAM6 and (c) PAM4 BER versus ROP for 200-m SMF transmission. Insets are selected eye diagrams.

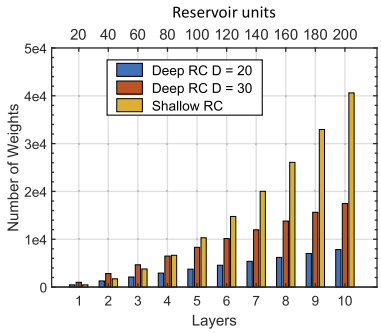

Fig. 5. Relationship between the number of weights and the number of reservoir units in shallow and deep RC.

Table 1. Comparison of Computational Complexity[a]

Methods	Total Number of Real Multiplications
DFE	N (68)
Shallow RC	$H\cdot(H+3)+2$ (6642)
Deep RC	$D^2\cdot(2L-1)+D\cdot(L+2)+2$ (2922)

[a] N, the total number of feedforward and feedback taps in the DFE; H, the total reservoir units of shallow RC; D, the reservoir units of each layer in deep RC; L, the number of layers of the deep RC; (*), the number of real multiplications in this work.

in shallow RC is much larger than in deep RC when the reservoir units are larger than 80. Compared with the shallow RC, the increase of reservoir units in deep RC can be achieved by adding multiple layers, and then the connections between two different layers are reduced. Considering 80 reservoir units for shallow RC and 20 reservoir units of four layers for deep RC in our study, the deep RC achieves an approximately 50% weight reduction without degrading the BER, indicating that the deep RC has lower computational complexity and is hardware friendly. In addition, the computational complexity between the DFE and RC schemes is discussed and shown in Table 1. The RC approaches are shown to be more complex than the DFE scheme [18]. However, the further BER performance improvement enabled by the RC schemes is of great significance in the optical unamplified short-reach communication system.

In conclusion, we have demonstrated an optical amplification-free deep RC-assisted high-baudrate transmission for intra-data center interconnections. Signals of 100 Gbaud PAM6 and 112 Gbaud PAM4 were successfully transmitted over a 200-m SMF link with the BER below 6.25% OH-HD-FEC limit. For the PAM6 transmission, approximately 1-dB ROP sensitivity enhancement for B2B and 200-m SMF transmission was achieved using both RC schemes. We also have reached the BER below the KP4-FEC limit for PAM4 over 200-m SMF transmission, thanks to improved transmission performance with RC schemes in the optical amplification-free link. The deep RC and shallow RC have comparable BER performance, whereas the hardware requirement of weights generation and storage in deep RC is lower than in shallow RC. We believe that the optical amplification-free deep RC-assisted high-baudrate IM/DD system has a promising application for the next generation of intra-data center communications.

Funding. National Natural Science Foundation of China (U2006217, 61775015); China Scholarship Council (202107090113); National Key Research and Development Program of China (2018YFB1801500); Vetenskapsrådet (2019-05197, 2022-04798); H2020 ICT TWILIGHT Project (781471); ERDF-Funded RINGO project (1.1.1.1/21/A/052); RTU Science Support Fund.

Disclosures. The authors declare no conflicts of interest.

Data availability. Data underlying the results presented in this paper are not publicly available at this time but may be obtained from the authors upon reasonable request.

REFERENCES

1. X. Pang, O. Ozolins, R. Lin, L. Zhang, A. Udalcovs, L. Xue, R. Schatz, U. Westergren, S. Xiao, W. Hu, G. Jacobsen, S. Popov, and J. Chen, J. Lightwave Technol. **38**, 492 (2020).
2. B. Sang, W. Zhou, Y. Tan, M. Kong, C. Wang, M. Wang, L. Zhao, J. Zhang, and J. Yu, J. Lightwave Technol. **40**, 2890 (2022).
3. K. Zou, Y. Zhu, and F. Zhang, J. Lightwave Technol. **35**, 1900 (2017).
4. K. Wang, M. Zhao, M. Kong, and J. Yu, IEEE Photonics J. **12**, 3200712 (2020).
5. Q. Hu, R. Borkowski, Y. Lefevre, J. Cho, F. Buchali, R. Bonk, K. Schuh, E. De Leo, P. Habegger, M. Destraz, N. Del Medico, H. Duran, V. Tedaldi, C. Funck, Y. Fedoryshyn, J. Leuthold, W. Heni, B. Baeuerle, and C. Hoessbacher, J. Lightwave Technol. **40**, 3338 (2022).
6. D. Che, Y. Matsui, R. Schatz, R. Rodes, F. Khan, M. Kwakernaak, and T. Sudo, J. Lightwave Technol. **39**, 845 (2021).
7. O. Ozolins, M. Joharifar, and T. Salgals, *et al.*, J. Lightwave Technol. **41**, 1200 (2023).
8. X. Pang, A. Udalcovs, R. Schatz, V. Bobrovs, G. Jacobsen, S. Popov, and O. Ozolins, IEEE Photonics Technol. Lett. **33**, 1046 (2021).
9. J. Zhang, L. Yan, L. Jiang, A. Yi, Y. Pan, W. Pan, and B. Luo, IEEE Photonics J. **13**, 3100106 (2021).
10. M. Han, M. Wang, N. Zhang, H. Mu, B. Wu, Y. Liu, and F. Yan, Opt. Fiber Technol. **53**, 102042 (2019).
11. K. Zhong, X. Zhou, J. Huo, C. Yu, C. Lu, and A. P. T. Lau, J. Lightwave Technol. **36**, 377 (2018).
12. G. S. Yadav, C. Y. Chuang, K. M. Feng, J. Chen, and Y. K. Chen, Opt. Lett. **46**, 1999 (2021).
13. S. Cai, M. Wang, M. Han, B. Wu, J. Sun, and J. Zhang, Appl. Opt. **61**, 3473 (2022).
14. A. Argyris, J. Bueno, and I. Fischer, Sci. Rep. **8**, 8487 (2018).
15. F. Da Ros, S. M. Ranzini, H. Bulow, and D. Zibar, IEEE J. Sel. Top. Quantum Electron. **26**, 7701912 (2020).
16. O. Ozolins, X. Pang, M. I. Olmedo, A. Kakkar, A. Udalcovs, S. Gaiarin, J. R. Navarro, K. M. Engenhardt, T. Asyngier, R. Schatz, J. Li, F. Nordwall, U. Westergren, D. Zibar, S. Popov, and G. Jacobsen, J. Lightwave Technol. **35**, 1174 (2017).
17. C. Gallicchio, A. Micheli, and L. Pedrelli, Neurocomputing **268**, 87 (2017).
18. Y. Hong, S. Deligiannidis, N. Taengnoi, K. R. H. Bottrill, N. K. Thipparapu, Y. Wang, J. K. Sahu, D. J. Richardson, C. Mesaritakis, A. Bogris, and P. Petropoulos, IEEE J. Sel. Top. Quantum Electron. **28**, 3700410 (2022).